J. Cent. South Univ. (2021) 28: 3800−3817
DOI: https://doi.org/10.1007/s11771-021-4764-0

Springer

Mechanical properties and microstructure evolution of an Al-Cu-Li alloy subjected to rolling and aging

WANG Lin(王琳)[1,2], BHATTA Laxman[1,2], XIONG Han-qing(熊汉青)[1,2],
LI Chang(李畅)[1,2], CUI Xiao-hui(崔晓辉)[1,2,3]*, KONG Charlie[4], YU Hai-liang(喻海良)[1,2,3]*

1. State Key Laboratory of High Performance Complex Manufacturing, Central South University, Changsha 410083, China;
2. College of Mechanical and Electrical Engineering, Central South University, Changsha 410083, China;
3. Light Alloys Research Institute, Central South University, Changsha 410083, China;
4. Electron Microscope Unit, University of New South Wales, Sydney, NSW 2052, Australia

Abstract: The mechanical properties and microstructure of Al-Cu-Li alloy sheets subjected to cryorolling (−100 °C, −190 °C) or hot rolling (400 °C) and subsequent aging at 160 °C for different times were investigated. The dynamic precipitation and dislocation characterizations were examined via transmission electron microscopy and X-ray diffraction. The grain morphologies and the fracture-surface morphologies were studied via optical microscopy and scanning electron microscopy. Samples subjected to cryorolling followed by aging exhibited relatively high dislocation densities and a large number of precipitates compared with hot-rolled samples. The samples cryorolled at −190 °C and then aged for 15 h presented the highest ultimate tensile strength (586 MPa), while the alloy processed via hot rolling followed by 10 h aging exhibited the highest uniform elongation rate (11.5%). The size of precipitates increased with the aging time, which has significant effects on the interaction mechanism between dislocations and precipitates. Bowing is the main interaction method between the deformation-induced dislocations and coarsened precipitates during tensile tests, leading to the decline of the mechanical properties of the alloy during overaging. These interesting findings can provide significant insights into the development of materials possessing both excellent strength and high ductility.

Key words: Al-Cu-Li alloy; cryorolling; artificial aging; dynamic precipitation; dislocation density; mechanical property

Cite this article as: WANG Lin, BHATTA Laxman, XIONG Han-qing, LI Chang, CUI Xiao-hui, KONG Charlie, YU Hai-liang. Mechanical properties and microstructure evolution ofan Al-Cu-Li alloy subjected to rolling and aging [J]. Journal of Central South University, 2021, 28(12): 3800−3817. DOI: https://doi.org/10.1007/s11771-021-4764-0.

1 Introduction

Aluminum-copper-lithium (Al-Cu-Li) alloys are ideal structural materials for aerospace and aircraft vehicles because of their high modulus, low density, excellent fatigue properties, and high strength-to-weight ratio [1−3]. Artificial aging is one of the most effective methods for improving the mechanical properties of Al-Cu-Li alloys [4]. The

Foundation item: Project(2019YFB2006500) supported by the National Key Research and Development Program, China; Project (51674303) supported by the National Natural Science Foundation of China; Project(2020GK2032) supported by Hunan High-tech Industry Science and Technology Innovation Leading Plan, China; Project (2018RS3015) supported by the Huxiang High-level Talent Gathering Project of Hunan Province, China; Project(2017YFA0700700) supported by the Ministry of Science & Technology of China; Project(2019CX006) supported by Innovation Driven Program of Central South University, China

Received date: 2021-01-08; **Accepted date:** 2021-08-02

Corresponding author: YU Hai-liang, PhD, Professor; E-mail: yuhailiang1980@tom.com, yuhailiang@csu.edu.cn; ORCID: https://orcid.org/0000-0001-7959-0717; CUI Xiao-hui, PhD, Associate Professor; E-mail: cuixh622@csu.edu.cn

precipitation sequence of the Al-Cu-Li alloy during aging has been extensively investigated [5], and different strengthening precipitates such as θ' (Al_2Cu), δ' (Al_3Li), and T_1 (Al_2CuLi) have been observed [6]. Li content has significant effects on the dominant strengthening phases of the aged alloy. LI et al [7] systematically investigated the evolution of the main precipitates and mechanical properties (including yield strength and work-hardening properties) of AA2050 artificially aged for up to 500 h, and a unified model to predict the mechanical performance was developed. RODGERS et al [8] found that 6% − 9% pre-stretch can effectively facilitate the nucleation of precipitates because of pre-strain induced dislocations in Al-Cu-Li alloys. TSIVOULAS et al [9] proposed that the matrix precipitation induced by pre-strain can further improve the mechanical properties. MA et al [10] proposed that pre-strain applied before natural aging suppresses the clustering mechanism, which can lead to lower alloy hardness and improved alloy strength without ductility loss while suffering from natural aging prior to artificial aging. Proper processing technologies are also widely utilized to improve the mechanical properties of alloys. The strength of AA2195 sample processed through cross-rolling was higher than that of those processed through unidirectional rolling, due to different textures under different intensities of shear bands formed during the rolling process [11].

The mechanical properties of alloys can be enhanced through severe plasticity deformation (SPD) techniques, including high-pressure torsion [12−14], equal channel angular pressing [15−17], accumulative roll bonding (ARB) [18−20], and cryorolling [21−22]. Of these techniques, cryorolling is particularly common during the fabrication of ultrafine-grained metallic sheets, due to its speed and functionality in processing large volumes of metals and alloys using existing industrial rolling structures [23 − 27]. Rolling at cryogenic temperatures leads to the partial suppression of dynamic recovery mechanisms to modify the work-hardening rate, and this increases the number of accumulated strains [28]. Cryorolling is the most widely utilized to continuously fabricate ultra-fine grain alloy sheets [29]. Dynamic recovery was partially suppressed and deformation-induced dislocations accumulated during processing progress.

In recent years, researchers have become interested in analyzing the mechanical properties of materials processed at liquid-nitrogen or liquid-helium temperatures. The increased strain hardening rate of the cryo-deformation alloy may have a great influence on the evolution of statistically stored dislocations and geometrically necessary dislocations and thus can significantly affect mechanical properties [30]. An increase in the yield strength is mainly attributed to the formation of lattice distortions before the tensile test at cryogenic temperatures. Likewise, an increase in strength and ductility is due to the increase in dislocations and nano-twins resulting from the low stacking-fault energy [31]. In addition, the suppression of the dislocation movement on the slip plane at liquid-nitrogen temperature has significant effects on the fatigue properties of the alloy [32]. YU et al [33] compared the microstructure evolution of an AA1060 alloy processed via ARB and a combination of ARB and cryorolling. The ductility and strength of the sheets processed via ARB-cryorolling were higher than those of the ARB-processed samples, due to the suppression of dislocation movements at cryogenic temperatures. WANG et al [34] investigated the effect of dislocations on an AA1060 alloy processed via ARB at cryogenic temperatures. They claimed that the gap between the dislocation boundaries decreased with increasing rolling passes, and that the initial cube orientation of the outside layer rotated to an r-cube orientation. The strength of the materials continuously increased due to texture changes.

Importantly, the increase in strength resulting from grain refinement is always accompanied by a loss in ductility. Thus, there is an urgent need to establish a strategy for improving the strength of grain-refined materials without sacrificing ductility. Aging treatment can further improve UTS, ductilities, elasticity modules, and creep behavior [35− 37]. The generation, development, movement, and interaction of dislocations occur during the plastic deformation of metals. The dislocations formed during the SPD are preferential nucleation sites for nanosized precipitates within refined grains [38]. This is an ideal method to resolve the popular

strength-ductility dilemma. MEI et al [39] successfully utilized a combination processing of cryorolling, warm rolling, and following aging treatment to improve the strength and ductility of Al alloy sheets simultaneously through regulating precipitates, dislocations, sub-grain boundaries. SHANMUGASUNDARAM et al [40] processed an Al-Cu (2219) alloy through cryorolling and subsequent annealing/aging treatment and obtained a maximum yield strength of 485 MPa, ultimate tensile strength of 540 MPa, and ductility of 11%. The enhancement in mechanical properties was attributed to the strengthening by grain refinement and precipitations. Moreover, SPD followed by subsequent aging is one of the most promising approaches for fabricating excellent balanced high strength and high ductility alloys in large-scale industrial applications [41, 42]. The high ultimate tensile strength of 608 MPa, yield strength of 575 MPa and good ductility of 8.2% were achieved due to a high density of dislocations and precipitations when the Al-Cu-Li alloy was cryorolled at liquid nitrogen temperature with the total reduction of 83% and subsequence aged at 160 °C for 32 h [43]. However, less attention has been paid to the variations in the mechanical properties and the evolution of the microstructure of the Al-Li alloy processed at different cryogenic temperatures and high temperatures followed by aging, systematically.

This paper analyzes the strengthening mechanisms for the mechanical properties of an Al-Cu-Li alloy via a concurrent strengthening strategy based on grain refinement and precipitations. The Al-Cu-Li sheets were subjected to hot rolling, cryorolling, and subsequent aging. The effects of grain refinement, precipitation, and dislocation accumulation on mechanical properties were studied.

2 Experimental procedures

A 2-mm-thick plate of self-melted Al-Cu-Li alloy was used in this study. The sheets were cut from the original material to dimensions of 60×100 mm using an electrical discharge machine. The chemical composition of the alloy is presented in Table 1. The composition was confirmed through an inductively coupled plasma-optical emission spectroscopy test.

Table 1 Chemical composition (wt%) of Al-Cu-Li alloy

Cu	Mg	Zn	Li	Ag	Mn	Zr	Al
3.37	0.80	0.51	0.49	0.31	0.25	0.22	93.1

Before the sheets were rolled, they were solution treated at 450 °C for 1 h, followed by water quenching. The rolling processes was carried out on a multifunctional four-roll mill platform with a maximum rolling force of 130 kN. The back-up roll diameter was 260 mm, and the work roll diameter was 80 mm, and the maximum rolling width was 300 mm. The rolling speed was 2.4 m/min. The rolling experiments were performed under dry-friction condition, and the work roll surfaces were smooth. Cryorolling at −100 °C (CR−100 °C) and −190 °C (CR−190 °C) and hot rolling at 400 °C (HR 400 °C) were performed. Before each pass of cryorolling, the sheets were placed in a cryogenic container for 8 min, while for hot rolling, they were placed in a heating furnace for 5 min. After six rolling passes, the alloy sheet thickness was about 0.7 mm. The rolling procedure is presented in Table 2. A few hours later, the rolled alloys were subsequently aged at 160 °C for different times (0−24 h).

The mechanical properties and the microstructure evolution of the sheets subjected to rolling and subsequent aging were investigated. Tensile tests were performed at a strain rate of 0.03 s^{-1} at room temperature on a Shimadzu AGS-5/10kN testing machine. The tensile test values were the average of five measurements. The morphology of the grains after processing was studied using the optical microscope (the platform of VHX-5000, made by Japan KEYENCE company) after the alloy samples were etched with

Table 2 Rolling procedure

Rolling pass	0	1	2	3	4	5	6
Thickness of rolled sheets/mm	2.00	1.68	1.41	1.18	0.99	0.83	0.70

Keller's reagent (1 mL HF (48%), 1.5 mL HCl (conc.), 2.5 mL HNO_3 (conc.), and 95 mL H_2O) for about 18 s on the RD-ND plane. The fracture surfaces were studied using a MIRA 3 LMU scanning electron microscope with an accelerating voltage of 20 kV. A Philips CM200 transmission electron microscope, with a field-emission gun operating at 200 kV, was used to examine the cross-section microstructures in the rolling direction. A Thermo Fisher Helios G4 PFIB was used to prepare the transmission electron microscopy (TEM) specimens via the in situ lift-out technique. The X-ray patterns were collected between 15° and 110° (2θ) at room temperature using a Bruker D8 Advance diffractometer with Cu K_α radiation and a step size of 0.05°. The dislocation density of all samples which were fabricated by different processing method is determined by analyzing the XRD patterns through Jade 6.5.

3 Results

3.1 Microstructure evolution

Rolling at different temperatures and subsequent aging at 160 °C produced uneven-grain-size materials. Figure 1 shows the alloy microstructures in the transverse direction processed at three rolling temperatures followed by aging for 5 h and 10 h. Elongated grains were formed during

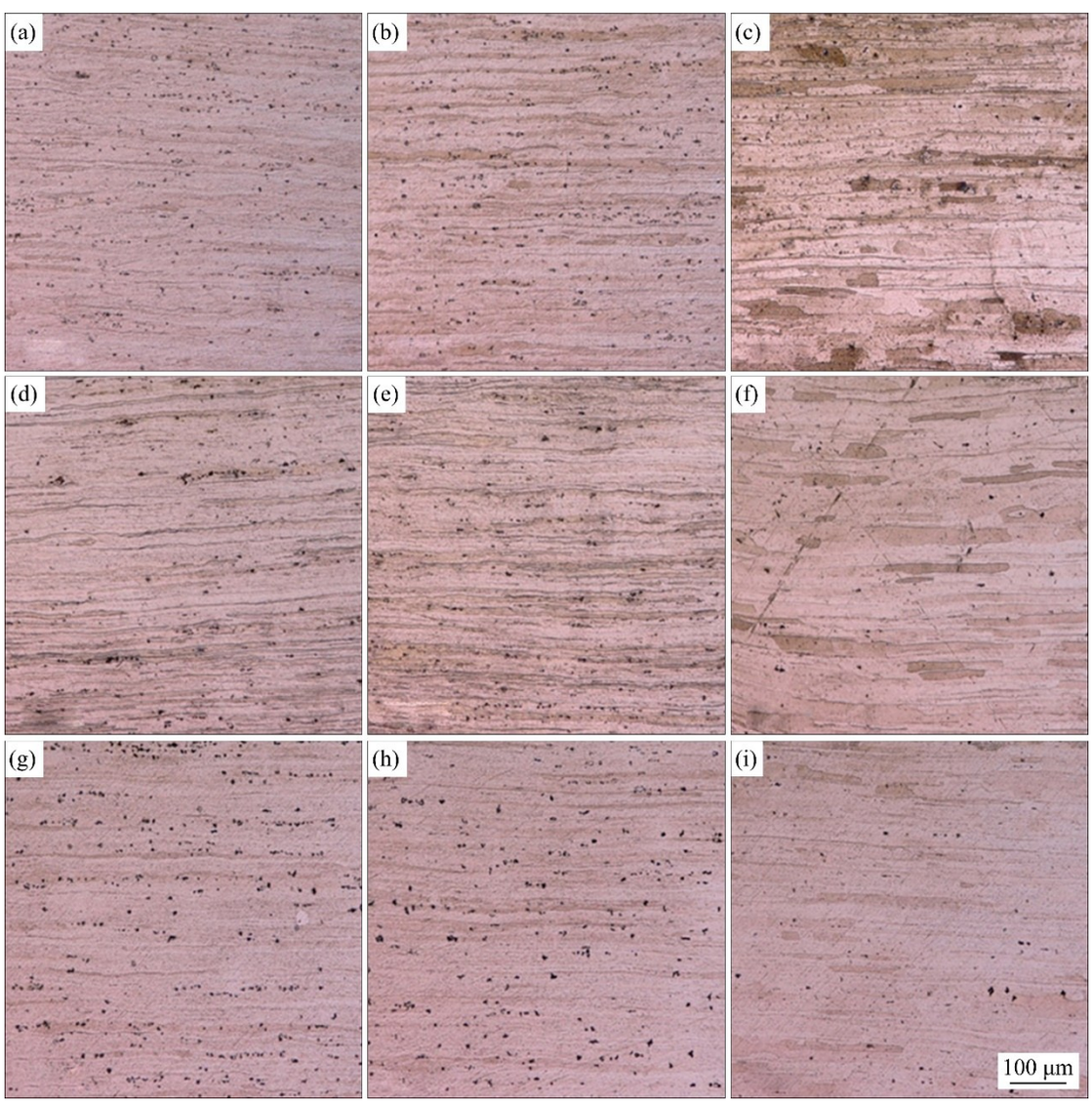

Figure 1 Microstructures of alloys subjected to (a) cryorolling (CR) at−190 °C, (b) CR−100 °C, (c) hot rolling (HR) at 400 °C, (d) CR −190 °C+5 h aging, (e) CR −100 °C+5 h aging, (f) HR 400 °C+5 h aging, (g) CR −190 °C+10 h aging, (h) CR −100 °C+10 h aging, and (i) HR 400 °C+10 h aging (Observed from TD in transverse direction)

the rolling deformation. Figure 1 shows that cryorolling produced more refined grain materials than hot rolling, and the grain size grew slightly with increasing aging time. The grain thickness of the rolled materials declined with decreasing rolling temperatures; this trend did not change during the ensuing aging stage. 100 grains were accounted from the optical microscope images and TEM images for grains size distribution. The grain size distribution of samples processed via cryorolling and hot rolling after the final pass are shown in Figure 2. The samples rolled at −100 °C and −190 °C showed average grain thicknesses of 3.17 and 2.62 μm, respectively. When the alloy was processed via hot rolling, an average grain thickness of 11.01 μm was observed, which is responsible for the low strength.

Figure 3 shows the TEM images of the samples. The grains were elongated along the rolling direction during rolling deformation at all temperatures, which agrees with the optical microscope images. Interestingly, the CR−100 °C-processed samples consisted of both coarse and fine grains (Figures 4(a) and (b)). The fine grains in the CR −190 °C-processed samples were relatively uniform. After the samples was rolled up to 65%, numerous dislocations were introduced within the grains and beside the grain boundaries. The dislocations were in the form of dislocation clusters or dislocation debris; these were newly formed with a size of <60 nm. A small fraction of the nano stacking fault was observed in the grains of all processed samples. Samples rolled at −190 °C had the highest stacking fault density among the rolled samples due to the stronger depressing effects for dynamic recovery and dislocation movement. The stacking fault density decreased with an increase in the rolling temperature.

During rolling deformation, the stacking fault piles up along the grain boundaries or beside the dislocation clusters (Figures 3(b), (d) and (f)). The increases in the rolling temperature from −190 °C to 400 °C offered more energy to the solute atoms to diffuse and cross the barriers. Moreover, the defects formed during the rolling process provided more precipitation nucleation sites [44]. These two factors greatly influenced the precipitation behavior during aging.

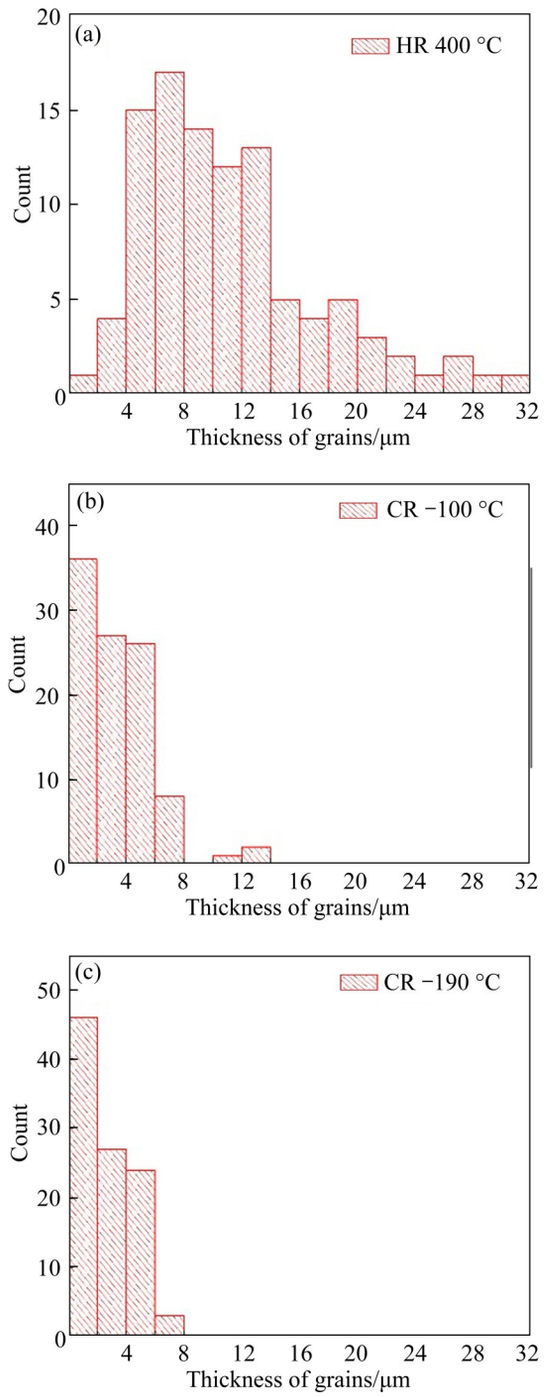

Figure 2 Grain thickness of alloys subjected to (a) HR 400 °C, (b) CR −100 °C, and (c) CR −190 °C after the final pass before aging (Observed from TD)

The effects of rolling temperature and aging time are illustrated in Figure 5. The dislocation density decreased with increasing aging time. The decrease in the dislocation density is attributed to the dislocation annihilation and dynamic recovery in the grains during aging. For the same aging time, the dislocation density of the alloy processed at

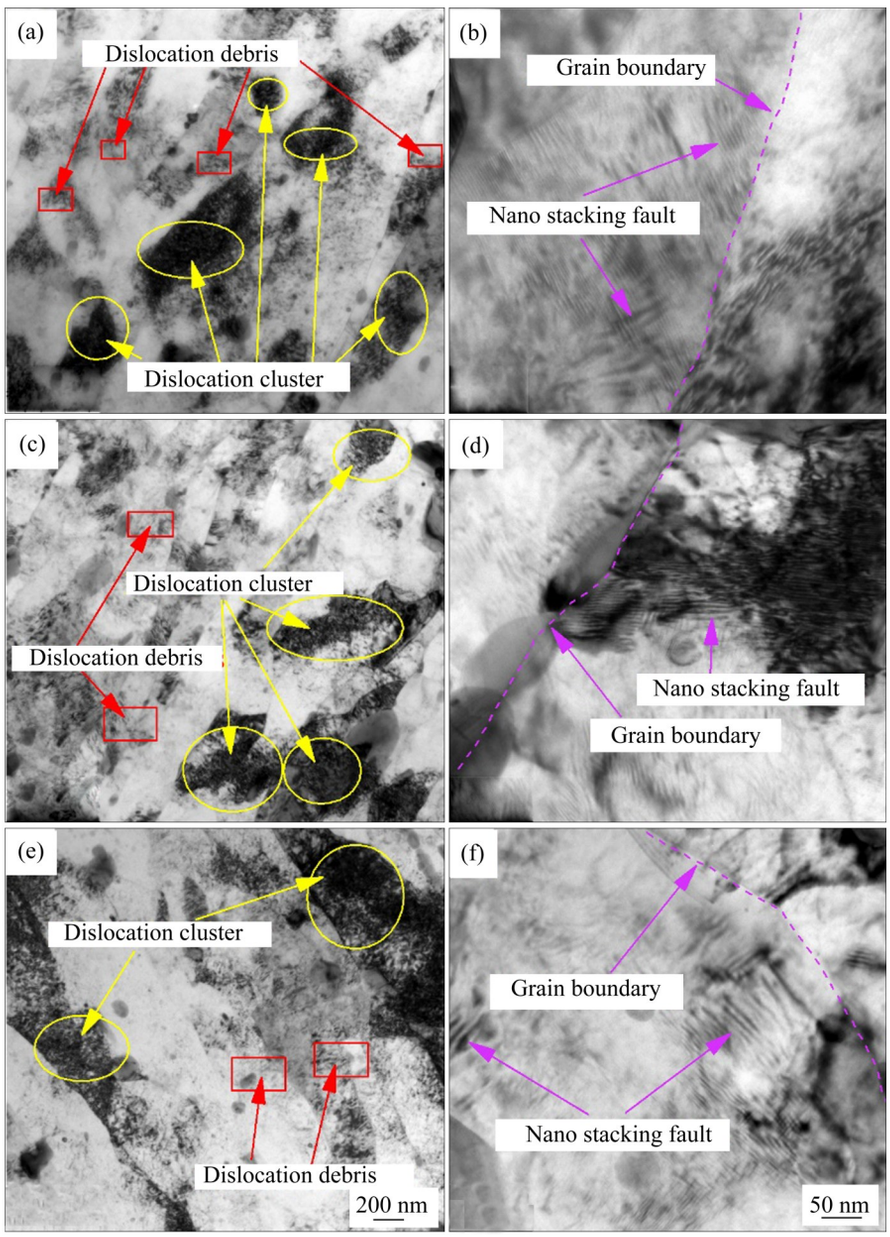

Figure 3 Transmission electron microscopy (TEM) images of the alloy subjected to (a, b) CR −190 °C, (c , d) CR −100 °C, and (e, f) HR 400 °C (Observed from TD)

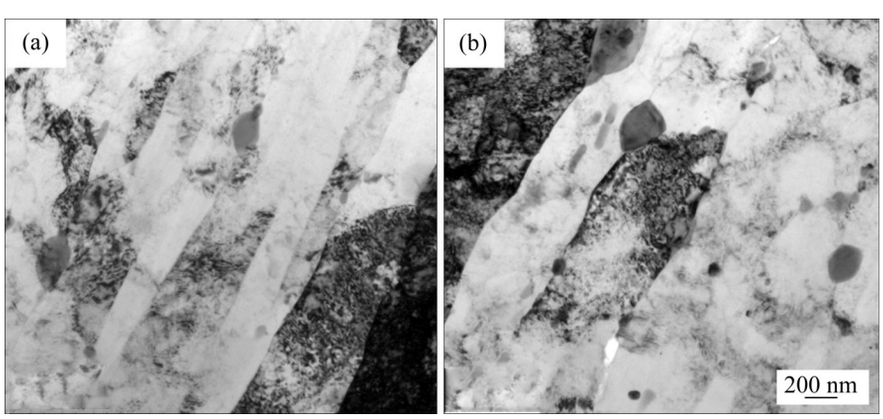

Figure 4 TEM images of alloy subjected to CR −100 °C: (a) Fine grain region; (b) Coarse grain region (Observed from TD)

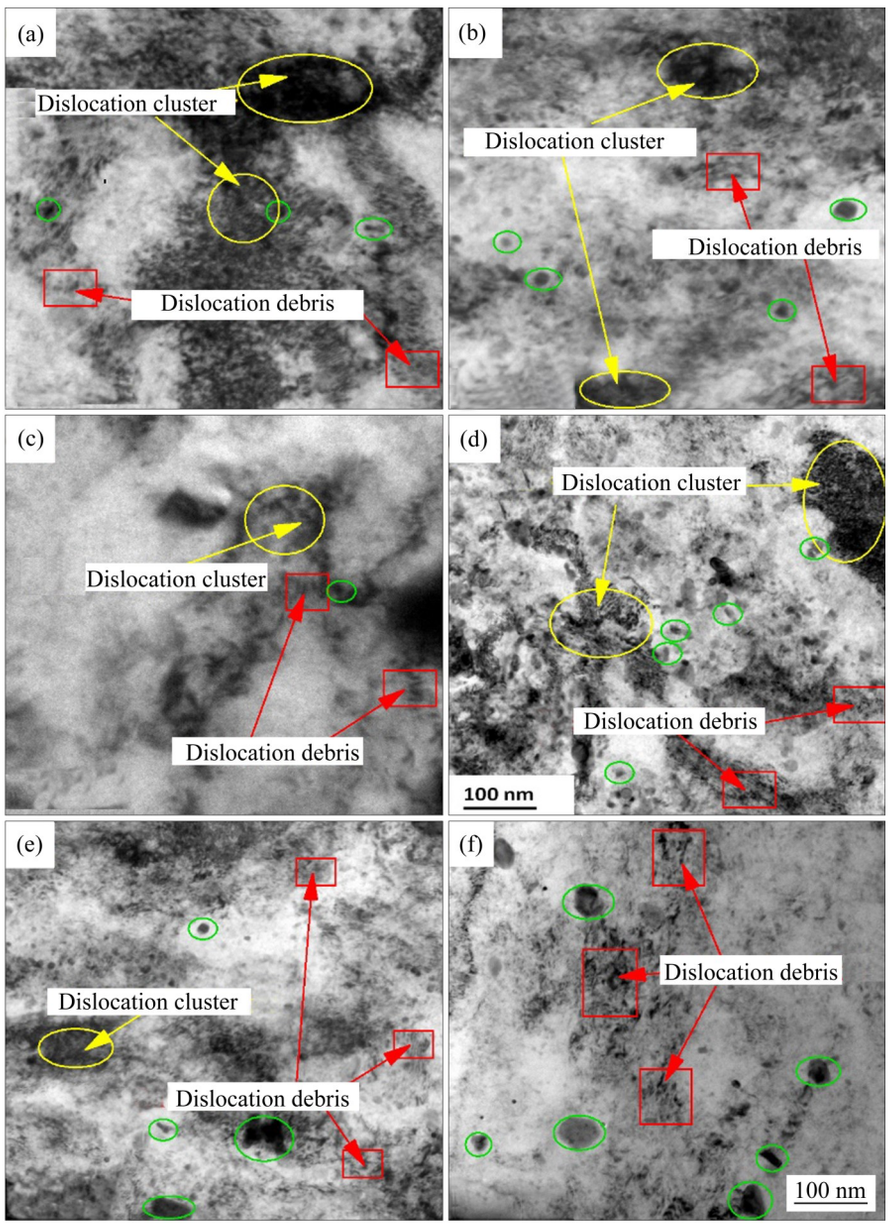

Figure 5 TEM images of alloy subjected to (a) CR −190 °C + 5 h aging, (b) CR −100 °C + 5 h aging, (c) HR 400 °C + 5 h aging, (d) CR −190 °C + 10 h aging, (e) CR −100 °C + 10 h aging, and (f) HR 400 °C + 10 h aging (Observed from TD)

− 190 ° C was the highest followed by the sample rolled at −100 °C, and then that rolled at 400 °C.

Moreover, the size of the precipitates varied with the aging time. After 5 h aging, θ phase with a size of approximately 40 nm and relatively low density was observed either in the grains or beside the dislocation clusters. An increase in the aging time to 10 h increased the density of the precipitates in the alloy. The size of the precipitates in the alloy rolled at 190 ° C and then aged for 10 h was relatively small. This may be due to the number of nucleation sites provided by the deformation-induced dislocations. Interestingly, the T_1 phase was not observed in the samples owing to the low lithium content in the alloy.

3.2 X-ray diffraction analysis

Figure 6 shows the X-ray diffraction pattern of the alloy subjected to different processing conditions. X-ray diffraction tests were performed to obtain the peak full width at half maximum which serves as input to Williamson-Hall equation

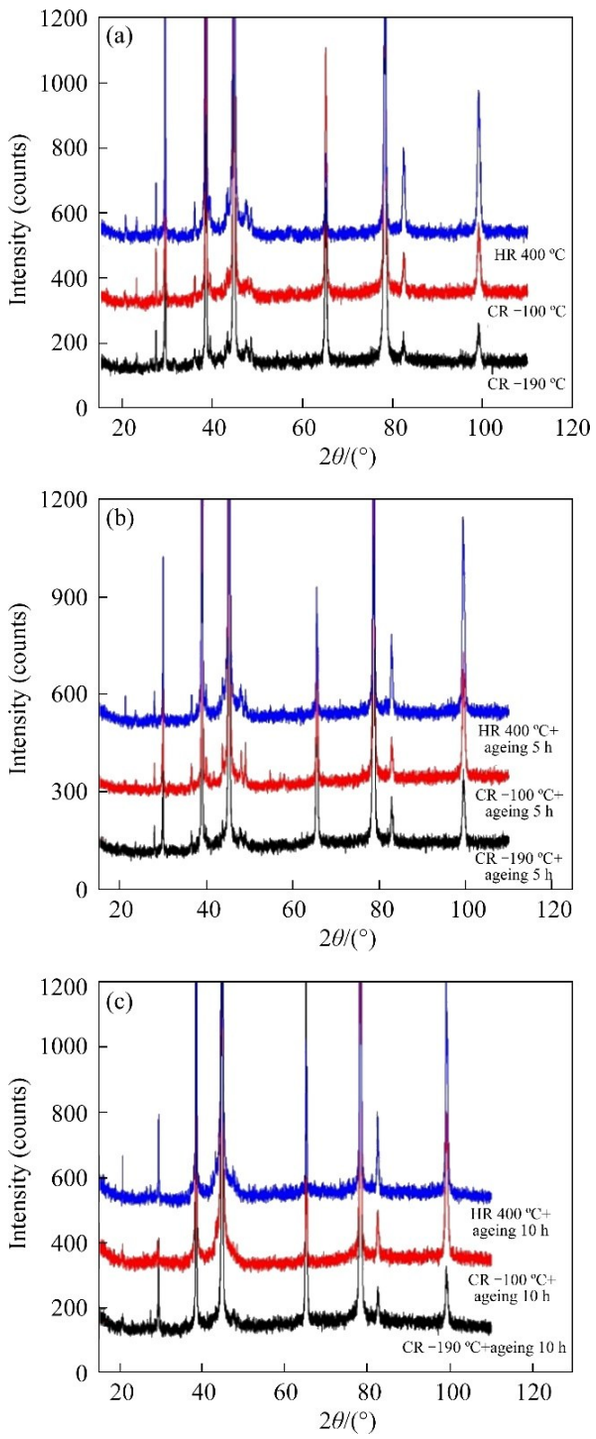

Figure 6 X-ray diffraction patterns of alloy: (a) Before aging; (b) After 5 h aging; (c) After 10 h aging

[45] to quantify the microstrain and dislocation density of samples at different processing conditions. The microstructure developed in the alloy was analyzed through the differences in the peak profiles such as peak broadening and peak shifting. The microstrain was obtained using Eq. (1) [46]:

$$B\cos\theta_b = \frac{\lambda K}{D} + \varepsilon \sin\theta_b \quad (1)$$

where B represents the width of the peak; θ_b represents the Bragg angle for the peak; λ represents the wavelength of the incident radiation; K is a constant; D is the average crystallite size; and ε is the sqrt of the average quadratic microstrain. After the domain size and microstrain were obtained, the dislocation density is computed from

$$\rho = \frac{2\sqrt{3}\,\varepsilon}{Db} \quad (2)$$

where b represents Burgers vector.

The microstrain and dislocation density are presented in Table 3. The CR −190 °C samples exhibited the highest dislocation density of 2.54×10^{14} m^{-2} owing to suppressions of dislocation movement and dynamic recovery. The density of dislocations sharply increased with decreasing rolling temperatures; the density of the HR 400 °C-processed samples was less than half of that of the CR −190 °C-processed samples. During aging treatment, the dislocation density of the alloy decreased with increasing aging time owing to dynamic recovery and dislocation annihilation. Even after 10 h of aging, the dislocation density in the alloy processed at cryogenic temperature is still over twice of that in the alloy processed at 400 °C, which is one of the reasons for the higher tensile strength and better ductility of the cryorolled samples.

3.3 Mechanical properties

Figure 7(a) shows the engineering tensile stress

Table 3 Lattice microstrain and dislocation density of alloy processed under different conditions

Process condition	Lattice strain/ 10^{-3}	Dislocation density/m^{-2}
CR −190 °C	2.42	2.54×10^{14}
CR −100 °C	2.34	2.37×10^{14}
HR 400 °C	1.61	1.12×10^{14}
CR −190 °C + aging 5 h	2.38	2.46×10^{14}
CR −100 °C + aging 5 h	2.25	2.20×10^{14}
HR 400 °C + aging 5 h	1.6	1.11×10^{14}
CR −190 °C + aging 10	2.35	2.39×10^{14}
CR −100 °C + aging 10 h	2.22	2.14×10^{14}
HR 400 °C + aging 10 h	1.52	1.00×10^{14}

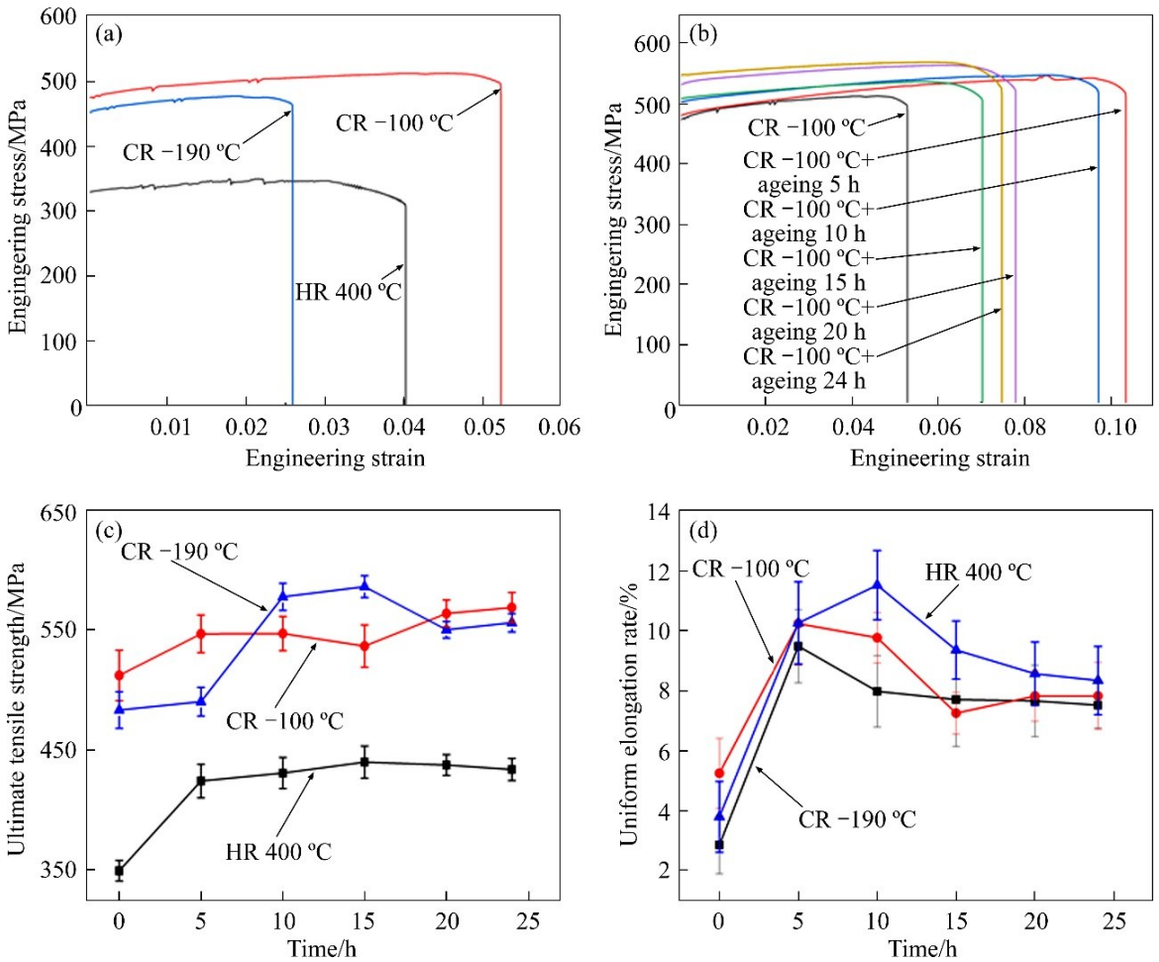

Figure 7 Mechanical properties of the sheets: (a) Engineering stress vs. strain curves after rolling at different temperatures; (b) Engineering stress vs strain curves of alloy cryorolled at −100 °C; (c) Ultimate tensile stress vs. aging time; (d) Uniform elongation rate vs. aging time

of the alloy processed at different conditions as a function of engineering strain tested at room temperature. The ultimate tensile strengths of the alloy rolled at these same temperatures were 350, 484 and 513 MPa, respectively. The uniform elongation rates of the alloy rolled at 400 ° C, −100 °C and −190 °C were 3.8%, 5.3% and 2.8%, respectively. Moreover, the samples rolled at 400 °C exhibited the lowest yield strength among all three rolling temperatures. A serrated flow behavior appeared during tensile tests for the samples after rolling, resulted from the interaction of numerous deformation-induced dislocations [47].

The mechanical properties of the alloy processed by cryorolled at −100 ° C and the subsequent aging for 5 – 24 h are illustrated in Figure 7(b) and the results of UTS and uniform elongation rates are summarized in Figures 7(c) and (d). Figure 7 shows that with increasing aging time, the UTS of the samples increased and then remained constant or decreased after attaining a peak value. The yield strength also followed the same trend. Likewise, the uniform elongation rate of the alloy processed at cryogenic temperatures rose after the first five hours ageing and then decreased with a further increase in aging time, while the peak uniform elongation rate of the hot rolled alloy was achieved after 15 h ageing. The UTS values of the samples rolled at 400 °C, −100 °C and −190 °C and then aged for 15 h was found as 440, 569 and 587 MPa, respectively. The peak uniform elongation rates of the samples rolled at 400 °C, −100 °C and −190 °C were 11.5%, 10.2% and 9.5%, respectively. We concluded that the microstructure evolution of the alloy during the first 10 h is significant for clarifying the strengthening mechanism.

3.4 Fracture surface analysis

Figures 8–10 show the fracture surface of the specimens at different rolling temperatures and aging times from different scales (500 and 20 μm). The fracture surface of the samples rolled at the different temperatures with ageing were flatter than the surfaces after 5 h ageing. The samples featured ductile and cleavage fractures, marked by yellow and red lines, respectively. Tearing ridges (marked by a pink line) were observed on the fracture surface. The tearing ridges were sharp in the alloy processed at −190 °C before aging. With the increase in rolling temperature, the tearing ridges decreased in number and gradually became parallel to the rolling direction. The dimples on the fracture surface of the samples subjected to high-temperature rolling followed by aging were slightly higher and deeper than those of the cryorolled and aged samples.

The voids on the fracture surface of the samples formed owing to the shedding of the second phase particles and enlargement of the voids during the tensile process. The samples rolled at 400 °C and then aged for 10 h presented the maximum number and depth of dimples on the fracture surface. Several studies have demonstrated that the occurrence of larger and deeper dimples on the fracture surface of the aluminum alloys enhances

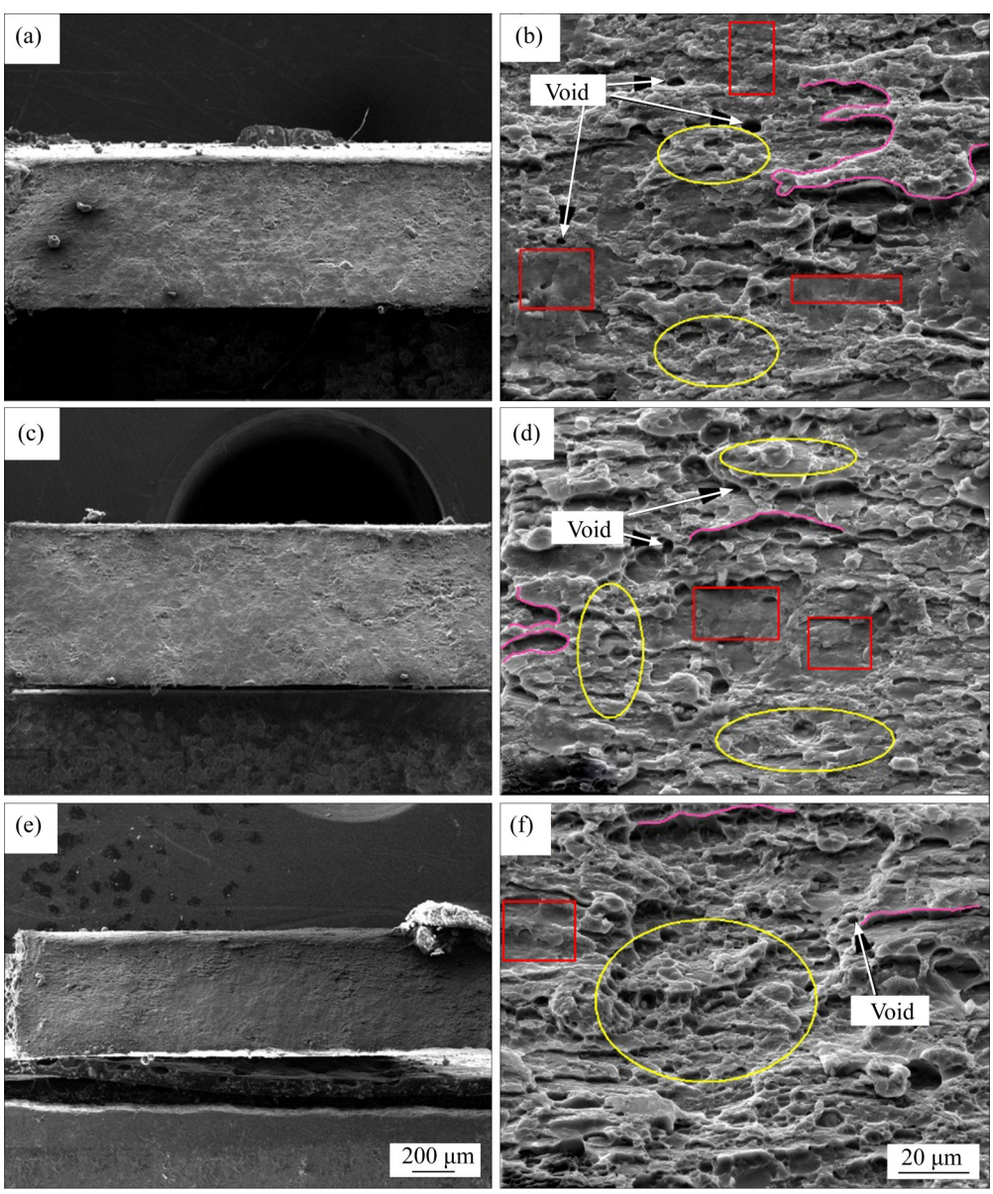

Figure 8 Scanning electron microscopy (SEM) images of fracture surfaces of alloy subjected to (a, b) CR −190 °C, (c, d) CR −100 °C, and (e, f) HR 400 °C

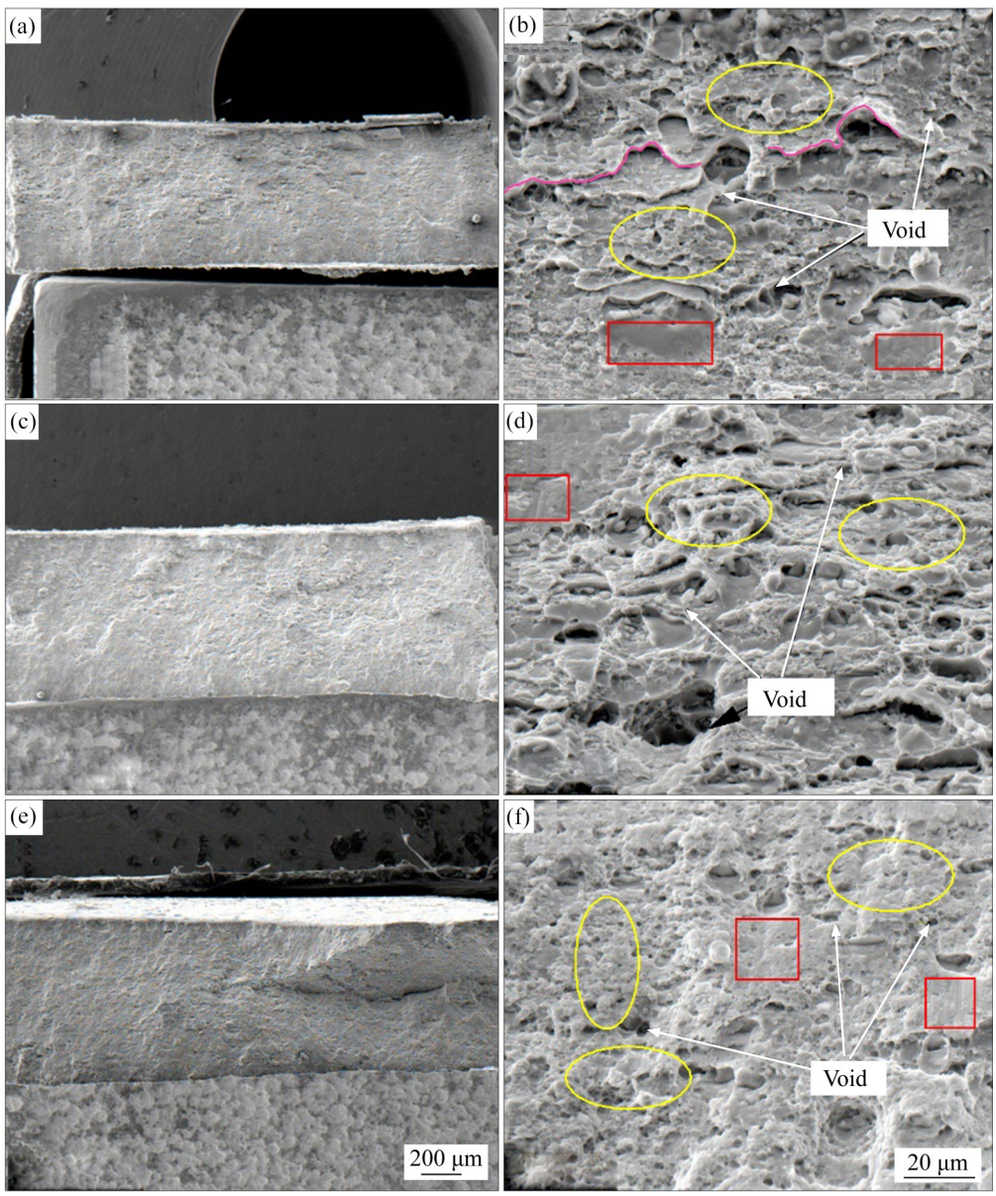

Figure 9 SEM images of fracture surfaces of alloy subjected to (a, b) CR −190 °C + 5 h aging, (c, d) CR −100 °C + 5 h aging, and (e, f) HR 400 °C + 5 h aging

the alloy ductility [48 – 49]. The fracture morphology observed in the current study agrees with the uniform elongation of the material processed under different conditions.

4 Discussion

4.1 Microstructure evolution mechanism during cryorolling and aging

In this study, alloy sheets were placed in a cryogenic environment to cool the alloy to the desired cryogenic temperature. One of the advantages of this approach is that rolling temperature can be precisely regulated by adjusting the nitrogen-flow speed. The dislocation density of the alloys before rolling was relatively low due to the solution treatment. Grain refinement and dislocation accumulation occurred during cryorolling and hot rolling. Numerous studies have shown that the strain-hardening rate of the cryorolled samples is lower than that of cold-rolled samples [50]. The dislocation density increases with a decrease of the rolling temperature leading to strong dislocation strengthening [51]. The deformation-induced dislocations provided numerous nucleation sites for precipitates during

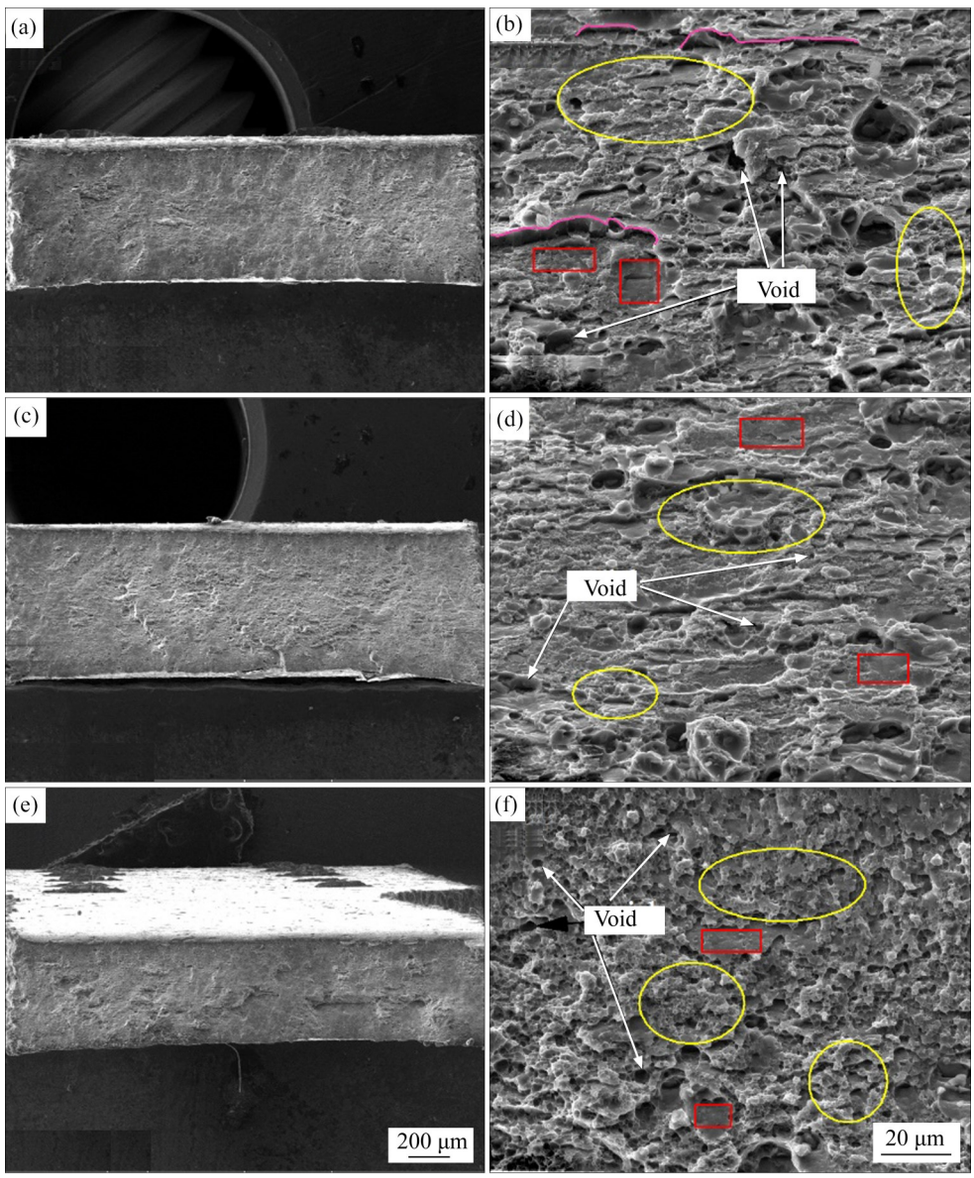

Figure 10 SEM images of fracture surfaces of alloy subjected to (a, b) CR −190 °C+10 h aging, (c, d) CR −100 °C+10 h aging, and (e, f) HR 400 °C+10 h aging

aging. The highest dislocation density of 2.54×10^{14} m^{-2}, which led to the highest peak UTS, was achieved when the alloy was cryorolled at −190 °C.

The dislocation movement was suppressed in cryorolled samples, leading to the accumulation and entanglement of dislocations. Therefore, dislocation clusters could more easily form during cryorolling process (Figure 3). During rolling deformation, the dislocation clusters were against the cross-slip formation, which induced the formation of nano-stacking faults of different concentrations in the alloy processed at different temperatures.

The cryorolled alloys showed extremely high strength owing to the refined grains and accumulation of dislocations [52]. Different from the uniform grain-distribution in the CR − 190 °C samples, coarse grains and fine grains occurred in the CR −100 °C-processed samples. In the samples processed via CR at −100 °C, high-angle boundaries between the neighboring grains were observed in the coarse grains; many dislocation clusters were observed in relatively coarse grains, whereas relatively-low density dislocations, primarily in the form of dislocation debris, occurred in fine grains. The dislocation debris was independent in grains. YOKOYAMA et al [32] reported a similar structure in Ti-Fe-O alloy.

With increasing aging time, the strengthening

of the Al_2Cu phase evolved from the Guinier-Preston zone [53]. The second phase gradually nucleated, grew, and coarsened during aging (Figure 5). The second phase significantly affected the interaction mechanism between dislocations and precipitates during the tensile test.

During tensile testing, the interaction mechanisms between the dislocations and precipitates with various sizes are different: The dislocation prefers the path that requires the least energy [47]. In this study, at aging times less than 5 h, the shearing between the dislocations and precipitates was the main interaction method owing to the small size of precipitates. Bowing became the dominant method with the coarsening of the precipitates. This leads to less resistance for hindering dislocation movements, as illustrated in Figure 11. Aging treatment after rolling resulted in a slight increase in the grain size due to the relatively high aging temperature (160 °C). Good balances between relatively high strength and good ductility was achieved for the alloys processed at −190 °C, −100 °C and 400 °C and then aged for 10 h, 5 h and 10 h, respectively. ZHANG et al [42] reported a similar result for the AA2195 alloy. The dislocation motion resistance caused by the interaction between deformation-induced dislocations and precipitates is defined as σ_{d-p}which would be utilized in the following analysis.

4.2 Strengthening mechanism of alloy during rolling and following aging

The strength of the rolled and then aged alloy can be calculated using Eq. (3) [54]:

$$\sigma_y = \sigma_{gb} + M_A\left[\tau_0 + \Delta\tau_s + \left(\Delta\tau_d^2 + \Delta\tau_p^2\right)^{\frac{1}{2}}\right] \quad (3)$$

Here σ_{gb} represents the strength from grain boundaries; M_A is the average Taylor factor; τ_0 is the critical resolved shear stress of pure aluminum; $\Delta\tau_s$ is the strength from solid solution; $\Delta\tau_d$ is the strength from dislocation; and $\Delta\tau_p$ is the strength from precipitation. The dislocation strengthening and precipitation strengthening can be neglected because of the extremely low dislocation density and the small number of precipitates in the alloy after solution heat treatment followed by water quenching.

Rolling increased the strength of σ_{d-d} between dislocations and σ_{d-g} between dislocations and precipitates leading to increased $\Delta\tau_d$. The precipitations were not observed in the samples before aging. Thus, $\Delta\tau_{s-SR400\,°C} = \Delta\tau_{s-SR-100\,°C} = \Delta\tau_{s-SR-190\,°C}$. Furthermore, the variation in the fibrous grain size led to $\sigma_{gb-SR400\,°C} < \sigma_{gb-SR-190\,°C} < \sigma_{gb-SR-100\,°C}$, suggesting that the excellent strain hardening of the heterogeneous structures can result in excellent strength and ductility [55].

LI et al [56] obtained the back stress that resulted from the strain partitioning during deformation through a storage model of geometrically necessary dislocations. The authors also proposed a mathematical model to calculate the strengthening effects of heterogeneous Cu.

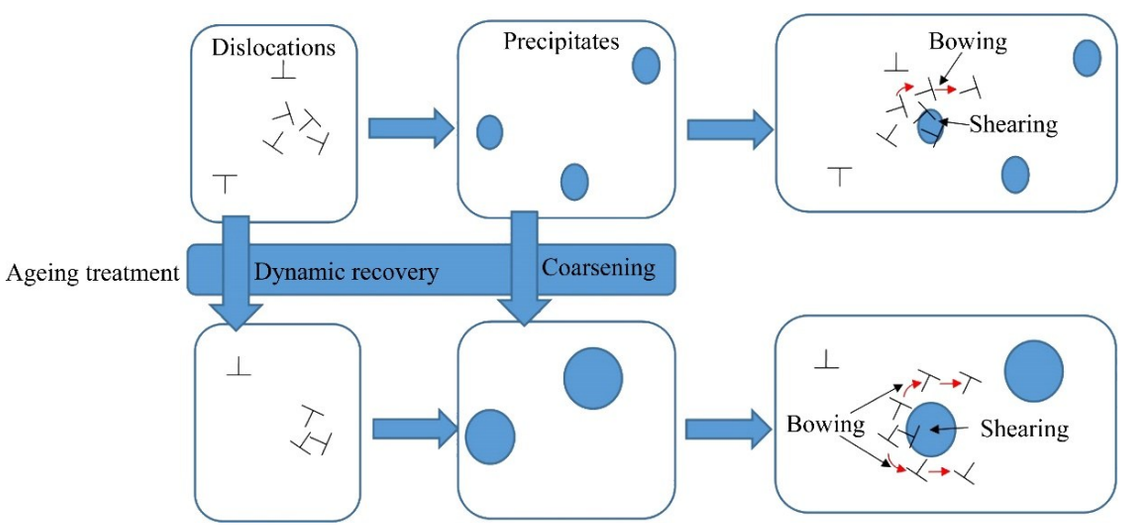

Figure 11 Schematic representation of interactions between dislocations and precipitates of different sizes during aging

However, this model is limited because it neglects the dislocations strengthening effects and shape effects of the inclusions. Moreover, different rolling parameters result in distinct deformation textures [57]. In the current study, the average Taylor factor M_A increased, and the rolling texture became stronger with a reduction of rolling temperature. Hence, the strength of the alloy after rolling at different temperatures can be obtained from Eq. (4):

$$\sigma_{\text{y - corres}} = \sigma_{\text{gb - corres}} + M_{\text{A - corres}} \cdot \left[\tau_0 + \Delta\tau_{\text{s - corre}} + \Delta\tau_{\text{d - corres}}\right] \quad (4)$$

Here the subscript " -corres" represents the corresponding rolling temperature. The increased dislocations, the increased average Taylor factor, and the refined grains led to a higher strength of the cryorolled alloy compared to high temperature rolled alloy. Likewise, the increase of the grain boundary strengthening from the special structure of CR −100 °C-processed alloy is greater than the effects from the decrease of dislocation strengthening and the average Taylor factor in the CR −190 °C-processed alloy. Hence, the strength of the CR −100 °C-processed alloy was slightly higher than that of the CR −190 °C-processed alloy.

During aging, the precipitation strengthening $\Delta\tau_{\text{p}}$ of all samples increased with nucleation, growth, and coarsening of precipitates, whereas the solid strengthening $\Delta\tau_s$ decreased. The annihilation and the dynamic recovery of dislocations led to a slight decrease of dislocation strengthening $\Delta\tau_{\text{d}}$. Furthermore, a minor increase of the average grain size contributed to a slight decrease in the grain boundary strengthening σ_{gb}. Moreover, the average Taylor factor decreased with increasing aging time. The alloy peak strength can be calculated via Eq. (5):

$$\sigma_{\text{y - corres}} = \sigma_{\text{gb - corres}} + M_{\text{A - corres}} \cdot \left[\tau_{\text{0 - corres}} + \left(\Delta\tau^2_{\text{d - corres}} + \Delta\tau^2_{\text{p - corres}}\right)^{\frac{1}{2}}\right] \quad (5)$$

The highest UTS (587 MPa) was obtained for the alloy rolled at −190 °C followed by subsequent aging for 15 h, due to the maximum precipitation strengthening $\Delta\tau_{\text{p - SR - 190 °C + ageing 15 h}}$. Figure 7(g) shows the effect of aging time on the ultimate tensile strength of the cryorolled and hot rolled alloy. And the UTS of the cryorolled alloy was greater than that of the high-temperature rolled alloy under all aging times. The first intersection of the curves of the CR −190 °C and −100 °C-processed samples occurred when the precipitation strengthening $\Delta\tau_{\text{p - SR - 190 °C + ageing}}$ of the CR −190 °C processed samples was higher than the sum of the precipitation strengthening $\Delta\tau_{\text{p - SR - 100 °C + ageing}}$of the CR −100 °C-processed samples; the difference of the grain boundary strengthening between them is expressed as $\Delta\sigma_{\text{gb}} = \sigma_{\text{gb - SR - 100 °C}} - \sigma_{\text{gb - SR - 190 °C}}$. Likewise, the second intersection occurred when the decrease of the precipitation strengthening of the CR −100 °C-processed alloy was greater than that of the CR −190 °C-processed alloy.

4.3 Ductility enhancement mechanism of alloy during rolling and following aging

In the present study, the uniform elongation rate of the alloy was specially discussed. The Burgers vector of the dislocation increased in grains with increasing deformation degree. The dislocation debris accumulated and piled-up near the original defect or sub-grain boundaries to form dislocation clusters. During tensile deformation, the interaction of the defects provided resistance against the plastic deformation. Moreover, the entangled and piled-up dislocations served as a major source of resistance during tensile test. Furthermore, a decrease in grain size provided several paths for microcrack propagation leading to a loss in ductility as the rolling temperature decreased from −100 °C to −190 °C. The deformation-induced special heterogeneous structure of the CR −100 °C samples is another important reason for its best ductility. This increase has been attributed to back stress [56].

After aging treatment, Cu atoms were gradually enriched, and the Al_2Cu phase was formed. During tensile test, the precipitates hindered the slip of dislocation clusters as displayed in Figure 11. Except for the change in the interaction mechanism between dislocations and precipitates, dislocations led to the stress concentration, which can easily lead to microcrack generation. The generation of microcracks contributed to a decrease in the stress until fracture during the tensile test. Moreover, the number of dislocations increased during the tensile test to significantly affect the alloy ductility.

The increase of ductility before peak aging can be discussed in two aspects. First, the hindrance of dislocation movement by precipitates delayed the dislocation cluster formation and the nucleation of dimples. Microcracks are generated on the precipitates of sufficient size [58]. Second, the increase in the precipitate volume fraction and the decline of the dislocations led to a uniform strain-distribution; these are indicated by the occurrence of numerous homogenous dimples [59, 60]. However, the alloy ductility decreased during over ageing due to a reduction in the dislocation accumulation ability, changes in the interaction mechanism between dislocations and precipitates, and the occurrence of slightly coarsened grains. As a result, the ductility of the rolled alloy increased with increased aging time until it reached its maximum value and then decreased.

5 Conclusions

This study investigated the mechanical properties and microstructure evolution of self-melted Al-Cu-Li alloy subjected to cryorolling (at −100 °C and −190 °C) and hot rolling (at 400 °C) followed by subsequent aging at 160 °C.

The cryorolled samples had higher tensile strength than the high-temperature-rolled samples without sacrificing ductility. This is because of the suppressions of dislocation movement and dynamic recovery during deformation at cryogenic temperatures, which leads to the accumulation and entanglement of dislocations. The −100 °C-rolled samples showed higher UTS values and better ductility than the −190 °C-rolled samples due to the special heterogeneous structure comprising fine grains and coarse grains.

The UTS and the uniform elongation rate of the samples aged at 160 °C after rolling first increased and then steadily decreased with increasing aging time. This behavior is attributed to the variation of the dislocation density, the precipitation, the interaction mechanism between the dislocations and the precipitates, and the average grain size. The samples cryorolled at −190 °C followed by 15 h aging exhibited the maximum tensile strength of 587 MPa.

References

[1] TRIOLO A, LIN J S, TRIOLO R. Early and late stages of demixing of a commercial Al-Li alloy [J]. Journal of Materials Science, 2002, 37(6): 1207−1213. DOI: 10.1023/A: 1014327824507.

[2] YUAN Shun, LI Yi-bo, HUANG Ming-hui, LI Jian. Determination of key parameters of Al–Li alloy adhesively bonded joints using cohesive zone model [J]. Journal of Central South University, 2018, 25(9): 2049−2057. DOI: 10.1007/s11771-018-3894-5.

[3] LIU F, LIU Z Y, LIU M, HU Y C, CHEN Y, BAI S. Analysis of empirical relation between microstructure, texture evolution and fatigue properties of an Al-Cu-Li alloy during different pre-deformation processes [J]. Materials Science and Engineering A, 2018, 726: 309−319. DOI: 10.1016/j.msea.2018.04.047.

[4] MUNOZ MORRIS M A, GUTIERREZ URRUTIA I, CALDERON N, MORRIS D G. Refinement of precipitates and deformation substructure in an Al-Cu-Li alloy during heavy rolling at elevated temperatures[J]. Materials Science and Engineering A, 2008, 492(1, 2): 268−275. DOI: 10.1016/j.msea.2008.03.036.

[5] DECRES B, DESCHAMPS A, DE GEUSER F, DONNADIEU P, SIGLI C, WEYLAND M. The influence of Cu/Li ratio on precipitation in Al-Cu-Li-X alloys [J]. Acta Materialia, 2013, 61(6): 2207−2218. DOI: 10.1016/j.actamat.2012.12.041.

[6] SIDHAR H, MISHRA R S. Aging kinetics of friction stir welded Al-Cu-Li-Mg-Ag and Al-Cu-Li-Mg alloys [J]. Materials and Design, 2016, 110: 60−71. DOI: 10.1016/j.matdes.2016.07.126.

[7] LI Y, SHI Z, LIN J. Experimental investigation and modelling of yield strength and work hardening behaviour of artificially aged Al-Cu-Li alloy [J]. Materials and Design, 2019, 183: 108121. DOI: 10.1016/j.matdes.2019.108121.

[8] RODGERS B I, PRANGNELL P B. Quantification of the influence of increased pre-stretching on microstructure-strength relationships in the Al-Cu-Li alloy AA2195 [J]. Acta Materialia, 2016, 108: 55−67. DOI: 10.1016/j.actamat.2016.02.017.

[9] TSIVOULAS D, PRANGNELL P B. Comparison of the effect of individual and combined Zr and Mn additions on the fracture behavior of Al-Cu-Li alloy AA2198 rolled sheet [J]. Metallurgical and Materials Transactions A, 2014, 45(3): 1338−1351. DOI: 10.1007/s11661-013-2103-2.

[10] MA P, ZHAN L, LIU C, WANG Q, LI H, LIU D, HU Z. Pre-strain-dependent natural ageing and its effect on subsequent artificial ageing of an Al-Cu-Li alloy [J]. Journal of Alloys and Compounds, 2019, 790: 8−19. DOI: 10.1016/j.jallcom.2019.03.072.

[11] NAYAN N, MISHRA S, PRAKASH A, MURTY S V S N, PRASAD M J N V, SAMAJDAR I. Effect of cross-rolling on microstructure and texture evolution and tensile behavior of aluminium-copper-lithium (AA2195) alloy [J]. Materials Science and Engineering A, 2019, 740−741: 252−261. DOI: 10.1016/j.msea.2018.10.089.

[12] ZHILYAEV A P, LANGDON T G. Using high-pressure torsion for metal processing: Fundamentals and applications

[J]. Progress in Materials Science, 2008, 53(6): 893 − 979. DOI: 10.1016/j.pmatsci.2008.03.002.

[13] VORHAUER A, PIPPAN R. On the homogeneity of deformation by high pressure torsion [J]. Scripta Materialia, 2004, 51(9): 921−925. DOI: 10.1016/j.scriptamat.2004.04.025.

[14] SUN Y, AINDOW M, HEBERT R J, LANGDON T G, LAVERNIA E J. High-pressure torsion-induced phase transformations and grain refinement in Al/Ti composites [J]. Journal of Materials Science, 2017, 52(20): 12170 − 12184. DOI: 10.1007/s10853-017-1331-z.

[15] VALIEV R Z, LANGDON T G. Principles of equal-channel angular pressing as a processing tool for grain refinement [J]. Progress in Materials Science, 2006, 51(7): 881 − 981. DOI: 10.1016/j.pmatsci.2006.02.003.

[16] DENG G Y, LU C, SU L H, TIEU A K, YU H L, LIU X H. Investigation of sample size effect on the deformation heterogeneity and texture development during equal channel angular pressing [J]. Computational Materials Science, 2013, 74: 75−85. DOI: 10.1016/j.commatsci.2013.03.007.

[17] LIU F, YUAN H, GOEL S, LIU Y, WANG J T. Bulk nanolaminated nickel: Preparation, microstructure, mechanical property, and thermal stability [J]. Metallurgical and Materials Transactions A, 2018, 49(2): 576 − 594. DOI: 10.1007/s11661-017-4394-1.

[18] TSUJI N, SAITO Y, LEE S H, MINAMINO Y. ARB (Accumulative Roll-Bonding) and other new techniques to produce bulk ultrafine grained materials [J]. Advanced Engineering Materials, 2003, 5(5): 338 − 344. DOI: 10.1002/adem.200310077.

[19] YU H, LU C, TIEU K, KONG C. Fabrication of nanostructured Aluminum sheets using four-layer accumulative roll bonding [J]. Materials and Manufacturing Processes, 2014, 29(4): 448 − 453. DOI: 10.1080/10426914.2013.872259.

[20] WANG H, SU L, YU H, LU C, TIEU K, LIU Y, ZHANG J.A new finite element model for multi-cycle accumulative roll bonding process and experiment verification[J]. Materials Science and Engineering A, 2018, 726: 93 − 101. DOI: 10.1016/j.msea.2018.04.040.

[21] YU H, DU Q, GODBOLE A, LU C, KONG C. Improvement in strength and ductility of asymmetric-cryorolled copper sheets under low-temperature annealing [J]. Metallurgical and Materials Transactions A, 2018, 49(10): 4398 − 4403. DOI: 10.1007/s11661-018-4700-6.

[22] YU H, YAN M, LI J, GODBOLE A, LU C, TIEU K, LI H, KONG C. Mechanical properties and microstructure of a Ti-6Al-4V alloy subjected to cold rolling, asymmetric rolling and asymmetric cryorolling [J]. Materials Science and Engineering A, 2018, 710: 10 − 16. DOI: 10.1016/j. msea. 2017.10.075.

[23] PANIGRAHI S K, JAYAGANTHAN R. A study on the mechanical properties of cryorolled Al − Mg − Si alloy [J]. Materials Science and Engineering A, 2008, 480(1, 2): 299−305. DOI: 10.1016/j.msea.2007.07.024.

[24] PANIGRAHI S K, JAYAGANTHAN R. Effect of ageing on microstructure and mechanical properties of bulk, cryorolled, and room temperature rolled Al 7075 alloy [J]. Journal of Alloys and Compounds, 2011, 509(40): 9609 − 9616. DOI: 10.1016/j.jallcom.2011.07.028.

[25] PANIGRAHI S K, JAYAGANTHAN R. Effect of annealing on precipitation, microstructural stability, and mechanical properties of cryorolled Al 6063 alloy [J]. Journal of Materials Science, 2010, 45(20): 5624−5636. DOI: 10.1007/s10853-010-4627-9.

[26] UI G G, SANG H L, WON J N. The evolution of microstructure and mechanical properties of a 5052 aluminum alloy by the application of cryogenic rolling and warm rolling [J]. Materials Transactions, 2009, 50(1): 82−86. DOI: 10.2320/matertrans.MD200801.

[27] YU H, LU C, TIEU K, LI H, GODBOLE A, ZHANG S. Special rolling techniques for improvement of mechanical properties of ultrafine-grained metal sheets: A review [J]. Advanced Engineering Materials, 2016, 18(5): 754 − 769. DOI: 10.1002/adem.201500369.

[28] GHOLINIA A. Processing to ultrafine grain structures by conventional routes [J]. Materials Science and Technology, 2000, 16(11, 12): 1251−1255. DOI: 10.1179/026708300101507316.

[29] XIONG H, SU L, KONG C, YU H. Development of high performance of Al alloys via cryo-forming: A review [J]. Advanced Engineering Materials, 2021, DOI: 10.1002/adem.202001533.

[30] HUGHES D A, HANSEN N, BAMMANN D J. Geometrically necessary boundaries, incidental dislocation boundaries and geometrically necessary dislocations [J]. Scripta Materialia, 2003, 48(22): 147 − 153. DOI: 10.1016/S1359-6462(02)00358-5.

[31] FU W, ZHENG W, HUANG Y, GUO F, JIANG S, XUE P, REN Y, FAN H, NING Z, SUN J. Cryogenic mechanical behaviors of CrMnFeCoNi high-entropy alloy [J]. Materials Science and Engineering A, 2020, 789: 139579. DOI: 10.1016/j.msea.2020.139579.

[32] YOKOYAMA H, UMEZAWA O, NAGAL K, SUZUKI T, KOKUBO K. Cyclic deformation, dislocation structure, and internal fatigue crack generation in a Ti-Fe-O alloy at liquid nitrogen temperature [J]. Metallurgical and Materials Transactions A, 2000, 31(11): 2793 − 2805. DOI: 10.1007/BF02830339.

[33] YU H, WANG H, LU C, TIEU A K, LI H, GODBOLE A, LIU X, KONG C, ZHAO X. Microstructure evolution of accumulative roll bonding processed pure aluminum during cryorolling [J]. Journal of Materials Research, 2016, 31(6): 797−805. DOI: 10.1557/jmr.2016.70.

[34] WANG Z J, MA M, QIU Z X, ZHANG J X, LIU W C. Microstructure, texture and mechanical properties of AA 1060 aluminum alloy processed by cryogenic accumulative roll bonding [J]. Materials Characterization, 2018, 139: 269−278. DOI: 10.1016/j.matchar.2018.03.016.

[35] TOPLOSKY V J, HAN K. Mechanical properties of cold-rolled and aged MP35N alloys for cryogenic magnet applications [J]. Advances in Cryogenic Engineering, 2012, 1435: 125−132. DOI: 10.1063/1.4712088.

[36] ZHOU C, ZHAN L H, SHEN R L, ZHAO X, YU H L, HUANG M H, LI H, YANG Y L, HU L B, LIU D B, HU Z G. Creep behavior and mechanical properties of Al-Li-S4 alloy at different aging temperatures [J]. Journal of Central South University, 2020, 27(4): 1168 − 1175. DOI: 10.1007/s11771-020-4357-3.

[37] XIE Yuan-kang, DENG Yun-lai, WANG Yu, GUO Xiao-bin. Effect of asymmetric rolling and subsequent ageing on the microstructure, texture and mechanical properties of the

Al-Cu-Li alloy [J]. Journal of Alloys and Compounds, 2020, 836: 155445. DOI: 10.1016/j.jallcom.2020.155445.

[38] LIU Dan-yang, LI Jin-feng, LIU Tian-le, MA Yun-long, IWAOKA H, HIROSAWA S, ZHANG Kai, ZHANG Rui-feng. Microstructure evolution and mechanical properties of Al-Cu-Li alloys with different rolling schedules and subsequent artificial ageing heat treatment [J]. Materials Characterization, 2020, 170: 110676. DOI: 10.1016/j.matchar.2020.110676.

[39] MEI L, CHEN X P, HUANG G J, LIU Q. Improvement of mechanical properties of a cryorolled Al-Mg-Si alloy through warm rolling and aging [J]. Journal of Alloy and Compounds, 2019, 777: 259–263. DOI: 10.1016/j.jallcom.2018.11.012.

[40] SHANMUGASUNDARAM T, MURTY B S, SUBRAMANYA SARMA V. Development of ultrafine grained high strength Al-Cu alloy by cryorolling [J]. Scripta Materialia, 2006, 54(12): 2013−2017. DOI: 10.1016/j.scriptamat.2006.03.012.

[41] HIROSAWA S, HAMAOKA T, HORITA Z, LEE S, MATSUDA K, TERADA D. Methods for designing concurrently strengthened severely deformed age-hardenable aluminum alloys by ultrafine-grained and precipitation hardenings [J]. Metallurgical and Materials Transactions A, 2013, 44(8): 3921−3933. DOI: 10.1007/s11661-013-1730-y.

[42] ZHANG C, LIU M, MENG Z, ZHANG Q, ZHAO G, CHEN L, ZHANG H, WANG J. Microstructure evolution and precipitation characteristics of spray-formed and subsequently extruded 2195 Al-Li alloy plate during solution and aging process[J]. Journal of Materials Processing Technology, 2020, 283: 116718. DOI: 10.1016/j.jmatprotec.2020.116718.

[43] DENG Yan-jun, HUANG Guang-jie, CAO Ling-fei, WU Xiao-dong, HUANG Li, XIA Ming-yong, LIU Qing. Improvement of strength and ductility of Al-Cu-Li alloy through cryogenic rolling followed by aging [J]. Transactions of Nonferrous Metals Society of China, 2017, 27(9): 1920−1927. DOI: 10.1016/S1003-6326(17)60216-4.

[44] LEE Y, DE-COOMAN B C. Characterization of compound particles formed during thin slab direct rolling of Ti-added Nb HSLA steel [J]. ISIJ International, 2014, 54(4): 893−899. DOI: 10.2355/isijinternational.54.893.

[45] SARKAR A, BHAWMIK A, SUWAS S. Microstructural characterization of ultrafine-grain interstitial-free steel by X-ray diffraction line profile analysis [J]. Applied Physics A, 2009, 94(4): 943−948. DOI: 10.1007/s00339-008-4870-y.

[46] JASEEM I, IMMANUEL J R, RAO P N, KHAN F, SAHOO B N, PANIGRAHI S K, KAMARAJ M. Synergetic effect of cryorolling and postroll aging on simultaneous increase in wear resistance and mechanical properties of an Al–Cu alloy [J]. Journal of Tribology, 2018, 140: 061607. DOI: 10.1115/1.4040162.

[47] GUPTA C, KUMAWAT B, CHAKRAVARTTY J K. Descriptors of temporal signatures of serrations in a low alloy steel [J]. Materials Science and Engineering A, 2015, 620: 407−410. DOI: 10.1016/j.msea.2014.10.032.

[48] KARAMOUZ M, AZARBARMAS M, EMAMY M, ALIPOUR M. Microstructure, hardness and tensile properties of A380 aluminum alloy with and without Li additions [J]. Materials Science and Engineering A, 2013, 582: 409−414. DOI: 10.1016/j.msea.2013.05.088.

[49] SHE X, JIANG X, ZHANG R, WANG P, TANG B, DU W. Study on microstructure and fracture characteristics of 5083 aluminum alloy thick plate [J]. Journal of Alloys and Compounds, 2020, 825: 153960. DOI: 10.1016/j.jallcom.2020.153960.

[50] CHANGELA K, NAIK H B, DESAI K P, RAVAL H K. Effect of rolling temperatures on mechanical and fracture behavior of AA 3003 alloy and pure Cu [J]. Applied Science, 2020, 2: 1109. DOI: 10.1007/s42452-020-2903-0.

[51] SRINIVAS B, PANIGRAHI S K.A phenomenological model based on nanostructured dislocation cluster interactions to predict the work hardening behavior of cryodeformed materials [J]. International Journal of Plasticity, 2020, 133: 102772. DOI: 10.1016/j.ijplas.2020.102772.

[52] GAIROLA S, JOSHI A, GANGIL B, RAWAT P, VERMA R. Correlation of tensile properties and fracture toughness with microstructural features for Al–Li 8090 alloy processed by cryorolling and post-rolled annealing [J]. Transactions of the Indian Institute of Metals, 2019, 72(7): 1743–1755. DOI: 10.1007/s12666-019-01641-z.

[53] DHAL A, PANIGRAHI S K, SHUNMUGAM M S. Precipitation phenomena, thermal stability and grain growth kinetics in an ultra-fine grained Al 2014 alloy after annealing treatment [J]. Journal of Alloys and Compounds, 2015, 649: 229−238. DOI: 10.1016/j.jallcom.2015.07.098.

[54] WANG Z, CHEN M, JIANG H, LI H, LI S. Effect of artificial ageing on strength and ductility of an Al-Cu-Mg-Mn alloy subjected to solutionizing and room-temperature rolling [J]. Materials Characterization, 2020, 165: 110383. DOI: 10.1016/j.matchar.2020.110383.

[55] WANG Y, GUO F, HE Q, SONG L, WANG M, HUANG A, LI Y, HUANG C. Synergetic deformation-induced extraordinary softening and hardening in gradient copper [J]. Materials Science and Engineering A, 2019, 752: 217–222. DOI: 10.1016/j.msea.2019.03.020.

[56] LI J, LU W, CHEN S, LIU C. Revealing extra strengthening and strain hardening in heterogeneous two-phase nanostructures [J]. International Journal of Plasticity, 2020, 126: 102626. DOI: 10.1016/j.ijplas.2019.11.005.

[57] SELVAN C C, NARAYANAN C S, RAVISANKAR B, NARAYANASAMY R, VALLIAMMAI C T. The dependence of the strain path on the microstructure, texture and mechanical properties of the cryogenic rolled Al-Cu alloy [J]. Materials Research Express, 2020, 7(3): 036525. DOI: 10.1088/2053-1591/ab7f9a.

[58] ROESCH L, HENRY G. Relationship between precipitation and dimple fracture in an 18 percent nickel maraging steel [C]// West Conshohocken, PA: ASTM, 1969: 3–32. DOI: 10.1520/STP47354S.

[59] JIANG H J, LIU C Y, ZHANG B, XUE P, MA Z Y, LUO K, MA M Z, LIU R P. Simultaneously improving mechanical properties and damping capacity of Al-Mg-Si alloy through friction stir processing [J]. Materials Characterization, 2017, 131: 425−430. DOI: 10.1016/j.matchar.2017.07.037.

[60] CHEN Y, LIU C Y, ZHANG B, QIN F C, HOU Y F. Precipitation behavior and mechanical properties of Al-Zn-Mg alloy with high Zn concentration [J]. Journal of Alloys and Compounds, 2020, 825: 154005. DOI: 10.1016/j.jallcom.2020.154005.

(Edited by YANG Hua)

中文导读

一种Al-Cu-Li合金轧制和时效的力学性能与微观组织演变

摘要：研究了深冷轧制(−100 °C，−190 °C)和热轧(400 °C)并随后在160 °C时效不同时间的Al-Cu-Li合金带材的力学性能和显微组织。通过透射电子显微镜和X射线衍射检查了动态析出和位错特征。通过超景深显微镜和扫描电子显微镜研究了微观组织和断口表面形貌。与热轧样品相比，经过深冷轧制和时效的样品表现出较高的位错密度和大量的析出物。在−190 °C深冷轧制后时效15 h的样品表现出最高的极限抗拉强度(586 MPa)，而通过热轧随后5 h时效处理的合金则表现出最高的均匀延展性(11.5%)。析出物的尺寸随着时效时间的增加而增加，这对位错与析出物之间的相互作用机理具有重要影响。过时效时，析出物尺寸比较粗大，拉伸变形过程中位错会绕过析出物进行运动，进而力学性能下降。

关键词：铝铜锂合金；深冷轧制；人工时效；析出；位错密度；力学性能